ROVIBRATIONAL SPECTRAL FINE STRUCTURE OF ICOSAHEDRAL MOLECULES

William G. HARTER and David E. WEEKS
Department of Physics, J. William Fulbright College, University of Arkansas, Fayetteville, AR 72701, USA

Received 26 August 1986

Predictions are made for possible spectral patterns in rovibronic fine structure in high-resolution spectra of icosahedrally symmetric molecules. Qualitative and semi-quantitative features are discussed which might help in identifying and assigning a complex spectrum. Interpretation of some features are made in terms of quantum and semi-classical dynamics.

Recently there have been reports of a number of molecular structures which may have icosahedral symmetry. These include the recently synthesized dodecahedrane [1] ($C_{20}H_{20}$), the tentatively identified [2] Buckminsterfullerene (C_{60}), as well as the better known [3] borohydride anion ($B_{12}H_{12}^{2-}$). While such highly symmetric structure is common in giant biochemical complexes such as virus heads, it is quite unusual to have icosahedral molecules which are amenable to gas phase infrared or Raman spectroscopy.

We give here a qualitative and semi-quantitative description of the possible rovibrational spectral structures which might be observed using laser diode, waveguide laser saturation absorption, or other high-resolution infrared or non-linear optical spectroscopic techniques. Certain spectral patterns and subpatterns might be expected to arise repeatedly. Their appearance would provide unmistakable evidence of icosahedral symmetry and aid greatly in spectral assignment and analysis of the molecular dynamics.

The spectral patterns described here are analogous to structures that have already been seen in other large spherical top molecules having tetrahedral, octahedral, or cubic symmetries. Laser spectra [4–6] of tetrafluoromethane (CF_4), sulfur hexafluoride (SF_6), and cubane (C_8H_8) exhibit prominent patterns and patterns within patterns which are called fine and superfine structure [7,8], respectively. The origin of these patterns can be simply related to the symmetry and rotational dynamics of the molecules in question [7,8]. The analysis of the octahedral spectral patterns is extended here to the icosahedral cases.

Rotational fine structure patterns occur in the eigenvalue spectrum of symmetric tensor operators represented in a $(2J+1)$-dimensional angular momentum basis for each value of total angular momentum J. The nature of the patterns becomes more evident as J increases. Some of the cubic patterns were first noticed by Lea, Leask and Wolf [9] for $J=6$–8. Later, more of the fine structure patterns were studied in computer generated tetrahedral tensor spectra up to $J=20$ by Dorney and Watson [10]. The detailed nature of the octahedral fine and superfine patterns up to $J=100$ was discussed by Fox et al. [11] and analyzed by Harter and Patterson [12].

The icosahedral spectral structure discussed here will be that found in the eigenvalue spectrum of the following sixth-rank operator:

$$T^{(6)} = \tfrac{1}{5}\sqrt{11}\,T^6_0 + \tfrac{1}{5}\sqrt{7}\,(T^6_5 - T^6_{-5})\,. \qquad (1)$$

This is the lowest-rank irreducible tensor operator having (non-trivially) icosahedral symmetry. (The next lowest icosahedral operator has tenth rank.) We are assuming here that (1) will play a role in icosahedral rovibrational Hamiltonians which is similar to that which octahedral fourth-rank tensor operators play in the SF_6 and C_8H_8 Hamiltonians.

An example of a numerically derived eigenvalue or level spectrum of (1) for $J=100$ is displayed in fig. 1. The computational methods are described in the appendix and in forthcoming works. In order to

0 009-2614/86/$ 03.50

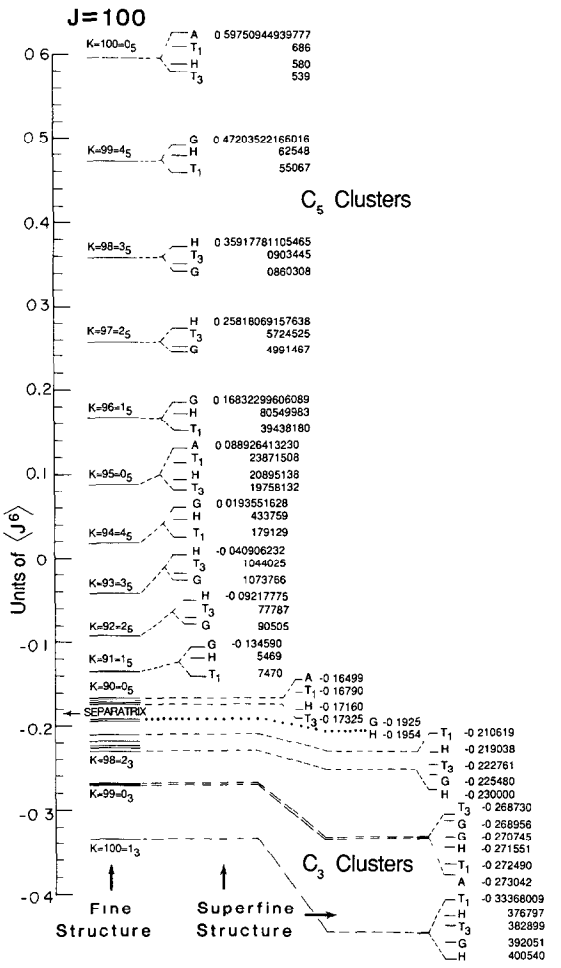

Fig. 1. Eigenvalue spectrum of 6th-rank icosahedral tensor operator $T^{(6)}$. Values are normalized by deleting a factor of $\langle J^6\rangle = [J(J+1)]^3$. The first significant digits of clustered eigenvalues which equal those of a top level are left blank in several cases.

understand the eigenvalue structure it is helpful to use a rotational energy (RE) surface [7,8] such as is drawn in fig. 2. The RE surface is a polar plot in energy–angular momentum space of a tensor Hamiltonian of the form

$$H = BJ^2 + t_{066}T^{(6)}\,, \qquad (2)$$

where B and t_{066} are the rotational and tensor distortion constants, respectively. For purposes of plotting, the constants are set arbitrarily to $B=1$ and $t_{066}=0.5$. The $T^{(6)}$ is expressed in terms of polar Euler

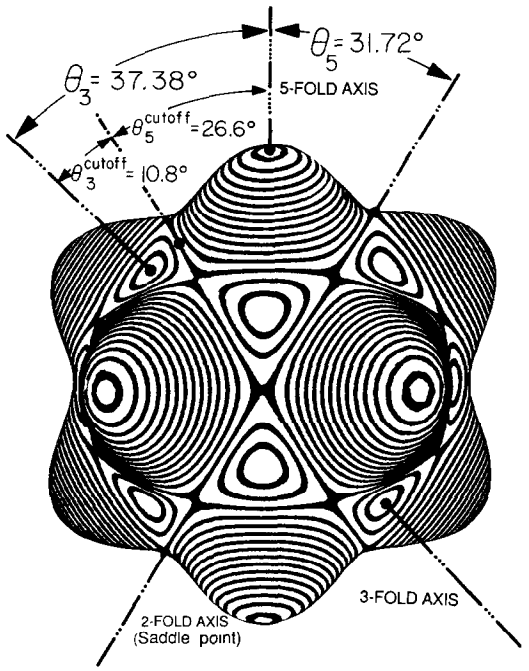

Fig. 2. Rotational energy (RE) surface for 6th-rank icosahedral tensor operator and energy level curves. 5-fold symmetry hill regions are copied 12 times and correspond to C_5 clusters of 12 levels in fig. 1. 3-fold valley regions correspond to C_3 clusters of 20 levels.

angles ($\phi=-\gamma$, $\theta=-\beta$) that define the direction of the classical J vector which is assumed to be fixed on the laboratory z axis of quantization [7],

$$\begin{aligned} T^6(\theta,\phi) = {}& \tfrac{1}{80}\sqrt{11}\,[(231\cos^6\theta \\ & -315\cos^4\theta + 105\cos^2\theta - 5) \\ & -42\cos\theta\sin^5\theta\cos\phi \\ & \times(16\cos^4\phi - 20\cos^2\phi + 5)]J^6\,. \end{aligned} \qquad (3)$$

As explained in refs. [7,8] the RE surface topography lines or level curves correspond to possible trajectories traced by the angular momentum vector $\boldsymbol{J}$ in the molecule-fixed frame. (RE surface energy is plotted radially as a function of $\boldsymbol{J}$ direction and the magnitude $|\boldsymbol{J}| \approx J$ is assumed constant for each surface.) Among all possible classical trajectories are a finite set of approximately $2J+1$ paths which satisfy certain quantization conditions. These quantizing level curves correspond to eigenlevels in the tensor spectrum.

Table 1

	(a) $C_3 \subset I$			(b) $C_5 \subset I$				
	0_3	1_3	2_3	0_5	1_5	2_5	3_5	4_5
A	1			1				
T_1	1	1	1	1	1			1
T_3	1	1	1	1		1	1	
G	2	1	1		1	1	1	1
H	1	2	2	1	1	1	1	1

One of the most noticeable features about the tensor level spectrum in fig. 1 is the grouping of levels belonging to different symmetry species into nearly degenerate clusters of 12 levels at high energies and 20 levels at low energies. Group representation theory of the icosahedral group I involves irreducible representations or symmetry species A, T_1, T_3, G, and H of degeneracy 1, 3, 3, 4, and 5, respectively. The much larger near-degeneracies of 12 or 20 correspond to 12 equivalent quantizing trajectories at a given energy on the RE-surface hills or to 20 equivalent valley trajectories belonging to the lowest energy levels.

As explained in ref. [7] the larger near-degeneracies are connected with *induced* representations. The 12-fold clusters are each labeled by one of the 12-dimensional representations $\{0_5\uparrow I,\ 1_5\uparrow I, ...,\ 4_5\uparrow I\}$ induced by irreducible representations 0_5, 1_5,..., or 4_5 of a local symmetry subgroup C_5. (The notation m_n refers to a wave with (m)modulo(n) wavelengths on the unit circle.) Similarly, the 20-fold clusters are labeled by 20-dimensional representations induced by 0_3, 1_3, or 2_3 of C_3. The connection between induced and irreducible representations and the key to determining the cluster structure is contained in simple correlation tables between I species and the species of C_3 or C_5 (see table 1).

For an example of the application of this table consider the highest cluster in fig. 1, which belongs to angular momentum component $K=J=100$ localized on a 5-fold symmetry axis through one of the 12 hills. Since this component is (0)mod(5) ($K=100=0_5$) it will give rise to 12 levels belonging to the I irreps contained in the 0_5 column of table 1b, i.e. A, T_1, T_3, and H. The second highest cluster in fig. 1 belongs to component $K=99=4_5$ and contains irreps T_1, G, and H in the 4_5 column. For the lowest energy components $K=J=100$ and 99 localized on the 3-fold symmetry axis there will be 20 level clusters of type 1_3 and 0_3, respectively. Cluster 1_3 has irreps T_1, T_3, G, and H (twice), while 0_3 has A, T_1, T_3, G (twice) and H. These clusters are indicated at the low end of the spectrum in fig. 1. There are fewer clusters of local symmetry C_3 than C_5 since the 3-fold symmetric valleys occupy a much smaller phase-energy space than the 5-fold hills.

The *inter*-cluster splitting in fig. 1 is called level fine structure while the (generally) much smaller *intra*-cluster splitting is called level superfine structure. The fine structure splittings are approximately equal to the classical precessional rates of the J vector at the corresponding energies. The superfine structure splittings are approximately proportional to quantum tunneling rates between wavepacket states localized on neighboring equivalent level curves. As explained in refs. [7,8], these tunneling rates decrease quasi-exponentially with increasing K, that is, when approaching hilltops or valley bottoms. Furthermore, a definite ordering and spacing of superfine structure patterns is predicted by assuming that only the nearest neighbor tunneling amplitude S is nonzero. The resulting predictions for superfine spacings and splittings are given in fig. 3. The predictions may be compared with the numerically derived results for $J=100$ given in fig. 1.

To do this we compare ratios of differences for neighboring eigenlevels. For example, the 0_5 cluster is predicted by fig. 3 to have tunneling ratios of

$$\frac{A-T_1}{T_1-H}=\frac{5-\sqrt{5}}{1+\sqrt{5}}=0.8541\,,$$

$$\frac{T_1-H}{H-T_3}=\frac{1+\sqrt{5}}{\sqrt{5}-1}=2.6180\,. \qquad (4)$$

The highest 0_5 cluster which can be readily resolved with IBM double precision is the $K=95=0_5$ cluster in fig. 1. The numerical ratios 0.8539 and 2.6177 agree to within about 0.01% with the simple formulas. The lowest 1_3 cluster is predicted by fig. 3 to have tunneling ratios that involve peculiar combinations of $\sqrt{5}$ and $\sqrt{13}$ as given by the following:

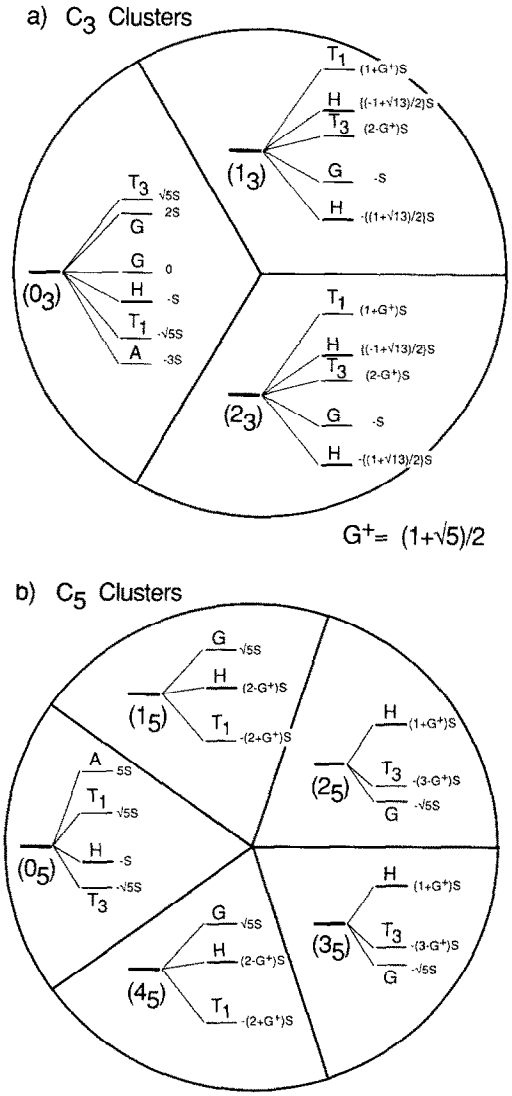

Fig. 3. Detailed superfine structure of (a) C_3 clusters and (b) C_5 clusters. Level splittings for each I-symmetry species is given relative to the cluster center of gravity in terms of its nearest neighbor tunneling amplitude S. Ordering is appropriate for even J, and is inverted for odd J.

$$\frac{T_1-H}{H-T_3}=\frac{4+\sqrt{5}-\sqrt{13}}{-4+\sqrt{5}+\sqrt{13}}=1.4284\,,$$

$$\frac{H-T_3}{T_3-G}=\frac{-4+\sqrt{5}-\sqrt{13}}{5-\sqrt{5}}=0.6663\,,$$

$$\frac{T_3-G}{G-H}=\frac{5-\sqrt{5}}{-1+\sqrt{13}}=1.0608\,. \qquad (5)$$

These predictions agree to within about 2% with the numerical ratios 1.440, 0.6666, and 1.078 derived from the computed levels at the bottom of fig. 1. We surmise that the poorer agreement for the C_3 clusters is due to higher-order tunneling caused by their trajectory confinement and close proximity to the boundary or separatrix between C_3 and C_5 levels.

The separatrix energy is just above the energy of the valley bottoms which are the sites of 3-fold symmetry axes as seen in fig. 2. In contrast, the hilltop sites for the 5-fold symmetry axes are much farther above the separatrix. The separatrix connects 30 saddle points which are sites of 2-fold symmetry axes. To compute the classical energy of the valleys, separatrix, or hilltops one may substitute the polar coordinates of any 3-fold, 2-fold, or 5-fold axis respectively, into (3) for $T^{(6)}(\theta,\phi)$. The results are

$$\begin{aligned}
T^{(6)}(\theta_3,\phi_3)&=T^{(6)}(37.38^\circ,0^\circ)\,,\\
&=-\tfrac{1}{5}\sqrt{11}J^6\,,\\
&=-0.36851\,J^6\,,\\
T^{(6)}(\theta_2,\phi_2)&=T^{(6)}(31.72^\circ,180^\circ)\,,\\
&=-\tfrac{1}{16}\sqrt{11}J^6\,,\\
&=-0.20729\,J^6\,,\\
T^{(6)}(\theta_5,\phi_5)&=T^{(6)}(0^\circ,0^\circ)\,,\\
&=\tfrac{1}{5}\sqrt{11}J^6\,,\\
&=0.66332\,J^6\,.
\end{aligned}$$

It is seen that the valley and hill energies bracket the low and high ends of the level spectrum in fig. 1, and that the separatrix energy is about where the level clusters dissolve from type C_3 into type C_5. In the separatrix region tunneling dominates and is indistinguishable from semi-classical precessional motion.

While separatrix levels may appear to be confused about their C_3 or C_5 identity, they still maintain a particular ordering *that is common to all regions of the spectrum*. The ordering was partly defined by the splitting predictions of either C_3 or C_5 given in fig. 3a or fig. 3b. This leads to a relatively simple "code wheel" shown in fig. 4. The wheel gives the order and qualitative form of icosahedral $T^{(6)}$ spectrum for *all values of J*. It is only necessary to calculate $(J)\mathrm{mod}(10)$ and $(J)\mathrm{mod}(6)$ and locate these num-

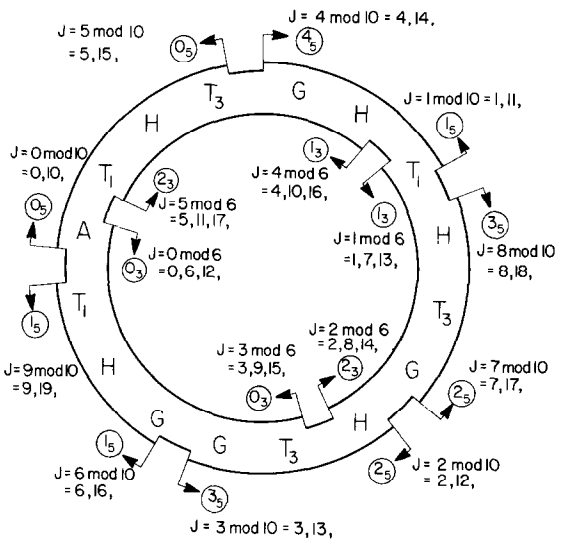

Fig. 4. Code ring for icosahedral symmetry content in angular momentum J levels. Ordering and clusterings of levels for $T^{(6)}$ Hamiltonian are indicated for all J. $J=30$ corresponds to one complete revolution plus an A singlet, and spans a 60-dimensional regular representation of I plus a scalar. Note that ordering for even J is opposite to that for odd J.

bers on the outside and inside arrows, respectively. The outside arrow indicates the beginning of the sequence starting from the highest level and points to which C_5 cluster that level belongs. The inside arrow does the same starting from lowest level in a C_3 cluster. For example, $J=24=(4)\mathrm{mod}(10)$ starts with 4_5 cluster (GHT_1) and ends at the $J=24=(0)\mathrm{mod}(6)$ arrow with a 0_3 cluster. The $J=24$ sequence would then be from top to bottom: $(GHT_1)_{4_5}$ $(HT_3G)_{3_5}$ $(H)(T_3GGHT_1A)_{0_3}$. Some clusters such as 0_3 in $J=24$ may be only partially formed if they are near the separatrix and some "loose levels" will always be present in this region. For low $J(J<12)$ most of the levels are unclustered, but *the ordering is always maintained.*

This concludes a preliminary description of the qualitative properties of icosahedral $T^{(6)}$ values. The quantitative properties depend upon molecular constants such as B and t_{066} for the vibrational ground state Hamiltonian (2) and a multitude of excited state parameters. The B values or inverse inertial constants are relatively easy to estimate and they provide an estimate of the equilibrium distribution of J values. For example, C_{60} is thought to have a radius of 3.5 Å. This leads to an estimated B value approximately 23 times that of SF_6. ($B_{SF_6}=0.091$ cm^{-1}, $r_{SF_6}=1.6$ Å.) The most populated J values of SF_6 are around $J=48$ at 300 K with the highest observed fine structure at $J\approx 150$. For C_{60} these numbers should be multiplied by $\sqrt{23}$ or almost 5.

The values of tensor parameters such as t_{066} are much more difficult to estimate since they depend upon vibrational anharmonicity. The fine structure splittings are proportional to products of the parameter with high powers of J, e.g. $t_{066}J^6$, $t_{246}J^4$, and so forth. This combined with a probability for high J values increases the likelihood for observing icosahedral fine structure.

A final point concerns the nuclear spin statistical weights and underlying hyperfine structure [13]. This will be discussed in future works. Preliminary results indicate that icosahedral structures with non-zero spins have relatively little variation of statistical weights from cluster to cluster. Complex cubic structures like cubane (C_8H_8) show this [8]. At the other extreme are spin-zero species such as C_{60} (assuming all carbon-12). This will be analogous to the tetrahedral osmium tetroxide OsO_4 in which only the clusters with A species show up. Finally, the spectroscopy and dynamics of slightly broken symmetry species like $^{12}C_{59}{}^{14}C$ would be extremely interesting.

We would like to thank Bill Ashmore for help in the computation using IBM ACRITH programs. This research was supported in part by National Science Foundation grant PHY-8696052 in theoretical physics.

Appendix

Exact numerical diagonalization or approximate calculation of $T^{(6)}$ fine structure uses matrix element formulas based on Wigner 3-j coefficients,

$$\langle {}^{J}_{M}|T^{6}_{q}|{}^{J}_{N}\rangle = C^{6JJ}_{qNM} = (-1)^{J-M}(2J+1)^{1/2}\begin{pmatrix} 6 & J & J \\ q & N & -M \end{pmatrix} . \tag{A1}$$

For $q=0$ (A1) are approximately the same as the $P^6(\cos\theta)$ Legendre polynomial,

$$\langle {}^{J}_{M}|T^{6}_{0}|{}^{J}_{N}\rangle \approx P^6(\cos\theta) , \quad \cos\theta = M/[J(J+1)]^{1/2} .$$

The necessary coefficients are as follows:

$$\begin{pmatrix} 6 & J & J \\ 0 & M & -M \end{pmatrix}$$

$$= (-1)^{J-M}\frac{-20(J+3{:}-2)+84M^2(5J^4+10J^3-20J^2-25J+14)-420M^4(3J^2+3J-7)+924M^6}{(2J+7{:}5)^{1/2}} , \tag{A2}$$

$$\begin{pmatrix} 6 & J & J \\ 5 & M & -(M+5) \end{pmatrix} = (-1)^{J-M}\frac{2M+J}{5!}\frac{11!(J-M+0{:}-4)(J+M+5{:}1)}{(2J+7{:}-5)} , \tag{A3}$$

where

$$(X+n{:}m) \equiv (X+n)(X+n-1)(X+n-2)...(X+m) . \tag{A4}$$

Combining (A2) with (1) gives the diagonal matrix elements ($M=K_5=N$) which are approximate 5-fold cluster level values,

$$\epsilon_{5\text{-fold}}(K_5) \approx \tfrac{1}{5}\sqrt{11}\langle {}^{J}_{K_5}|T^{6}_{0}|{}^{J}_{K_5}\rangle , \quad K_5 = J, J-1, J-2, ... \geqslant [J(J+1)]^{1/2}\cos(26.57°) . \tag{A5}$$

Approximate 3-fold values are

$$\epsilon_{3\text{-fold}}(K_3) \approx \tfrac{1}{5}\sqrt{11}\langle {}^{J}_{K_3}|T^{6}_{0}|{}^{J}_{K_3}\rangle , \quad K_3 = J, J-1, J-2, ... \geqslant [J(J+1)]^{1/2}\cos(10.81°) . \tag{A6}$$

Approximate K-cutoff angles are determined by separatrix angles on RE surface [7]. For $J=100$ the cutoff predictions are $K_5^{\text{cutoff}}=90$ and $K_3^{\text{cutoff}}=99$. This is confirmed by fig. 1.

References

[1] L.A. Paquette, R.J. Ternansky, D.W. Balough and G. Kentgen, J. Am. Chem. Soc. 105 (1983) 5446.

[2] H.W. Kroto, J.R. Heath, S.C. O'Brien, R.F. Curl and R.E. Smalley, Nature 318 (1985) 162.

[3] J.A. Wunderlich and W.N. Lipscomb, J. Am. Chem. Soc. 82 (1960) 4427.

[4] R.S. McDowell, in: Laser spectroscopy, Vol. 3, eds. J.L. Hall and J.L. Carlsten (Springer, Berlin, 1977) p. 102;
W.G. Harter and C.W. Patterson, Phys. Rev. A19 (1979) 2278.

[5] K.C. Kin, W.B. Person, P. Seitz and B.J. Krohn, J. Mol. Spectry. 76 (1979) 322;
J. Bordé and Ch. J. Bordé, Chem. Phys. 71 (1982) 417.

[6] A.S. Pine, A.G. Maki, A.G. Robiette, B.J. Krohn, J.K.G. Watson and Th. Urbanek, J. Am. Chem. Soc. 106 (1984) 891.

[7] W.G. Harter and C.W. Patterson, J. Chem. Phys. 80 (1984) 4241.

[8] W.G. Harter, J. Stat. Phys. 36 (1984) 749.

[9] K.R. Lea, M.J.M. Leask and W.P. Wolf, J. Phys. Chem. Solids 23 (1962) 1381.

[10] A.J. Dorney and J.K.G. Watson, J. Mol. Spectry. 42 (1972) 1.

[11] K. Fox, H.W. Galbraith, B.J. Krohn and J.D. Louck, Phys. Rev. A15 (1977) 1363.

[12] W.G. Harter and C.W. Patterson, J. Chem. Phys. 66 (1977) 4872; Phys. Rev. Letters 38 (1977) 224.

[13] W.G. Harter, Phys. Rev. A24 (1981) 192.